Pramana – J. Phys. (2019) 93:101
https://doi.org/10.1007/s12043-019-1855-7

Global stability analysis of axisymmetric boundary layer: Effect of axisymmetric forebody shapes

RAMESH BHORANIYA[1],* and VINOD NARAYANAN[2]

[1]Department of Mechanical Engineering, Marwadi Eduation Foundation Group of Institutions, Rajkot 360 003, India
[2]Department of Mechanical Engineering, Indian Institute of Technology, Palaj, Gandhinagar 382 355, India
*Corresponding author. E-mail: rameshkumar.bhoraniya@marwadieducation.edu.in

MS received 13 October 2018; revised 20 March 2019; accepted 18 July 2019

Abstract. This paper presents the effect of axisymmetric forebody shapes on the global stability characteristics of axisymmetric boundary layer developed on a circular cylinder. Axisymmetric forebodies like sharp-cone, ellipsoid, and paraboloid with a fineness ratio (FR) of 2.5, 5.0 and 7.5 are considered. The boundary layer starts to develop at a stagnation point on the forebody geometry and grows in spatial directions. The inflow velocity component is parallel to the axis of the cylinder, and hence the angle of attack is zero. The base flow is axisymmetric, non-parallel and non-similar. The linearised Navier–Stokes equations are derived in the cylindrical polar coordinates for the disturbance flow components. The discretised linearised Navier–Stokes equations along with appropriate boundary conditions form a general eigenvalue problem and it has been solved using Arnoldi's algorithm. The global temporal modes have been computed by solving the two-dimensional eigenvalue problem. The extent of a favourable pressure gradient developed in streamwise direction depends on the shape of axisymmetric forebody. The temporal and spatial growth of the disturbances has been computed for axisymmetric ($N = 0$) mode for different Reynolds numbers (Re). The forebody shapes have a significant effect on the base flow and stability characteristics at low Re.

Keywords. Forebody; global stability; axisymmetric; boundary layer.

PACS Nos **47.20.Ft; 47.20.Ib; 47.20.−k**

1. Introduction

This paper presents the effect of axisymmetric forebody shapes on the global stability characteristics of axisymmetric boundary layer. The development of viscous boundary layer on the nose of axisymmetric bodies starts from the stagnation point as a steady laminar flow growing in thickness along the streamwise direction until it becomes unstable or a transition to turbulence takes place. At the transition point, the growth of the downstream boundary layer is such that it exceeds the critical Reynolds number (Re). The stability analysis computations perform this task as accurate as possible. Based on this interpretation, to delay the transition, maintain a boundary layer as thin as possible and provide external flow environment with the strongly favourable pressure gradient. The growth of the boundary layer strongly depends on Re compared to the pressure gradient parameter, and so sometimes at higher Re even in favourable pressure gradient region transition takes place. Thus, the strategy of maximising the extent of laminar boundary layer reduces the drag forces on the axisymmetric propulsive bodies [1]. Narayanan and Govindarajan [2] studied the connection between the boundary layer instability and the birth of the turbulent spot and they found that at low noise level the Tollmien–Schlichting (TS) route is followed while at higher noise level bypass route is more likely followed. The turbulent spot birth depends on the pattern of secondary instability in either of the route. Casarella *et al* [3] found that the blunter the body shape is, the less is the extent of a favourable pressure gradient. As studied by Parson and Goodson [1] the purpose of delaying transition is to maximise the extent of laminar boundary layer to reduce the drag forces on the axisymmetric shapes of propulsive bodies like submarines, torpedoes, missiles, rockets, etc. A guided aerodynamic vehicle like missile needs to control the trajectory for its targets where aerodynamic stability is essential. Axisymmetric natural laminar flow bodies have minimum drag and permit long run of laminar flow. It is always expected in the design of fuselage, missile, torpedoes, submarine, etc.

Published online: 15 October 2019

to have a minimum drag for energy efficiency. James *et al* [4] and Holmes *et al* [5] have demonstrated in recent flight test that long run of laminar boundary layer flow can be achieved on the region of favourable pressure gradient on smooth airplane surface and provide a significant reduction in the drag. Past research has received little attention on fuselage shaping design to get natural laminar flow in open literature except for sail-plain body and hydrodynamic bodies. Carmichael [6] performed experiments on the NACA-66 airfoil about a longitudinal axis with a low fineness ratio (FR). The results indicate that a low FR and proper shape can produce a robust favourable pressure gradient on the forebody. As a result, the boundary layer remains laminar over a considerable length of the body. The pointed shaped bodies with hyperbolic or parabolic noses may offer less drag than the rounded or elliptic-nosed shapes. Many researchers have studied the base flow field around the bodies of revolution which is having practical applications in the field of aerodynamics and marine hydrodynamics such as fuselages, rockets, missiles, submarines, ship hulls, torpedoes, etc. for drag reduction and energy efficiency. Theofilis [7], Alizard and Robinet [8] and Akervik *et al* [9] have solved the two-dimensional eigenvalue problem numerically to study the temporal and spatial stability properties of the boundary layers. Rao [10], Tutty and Price [11] and Narayanan [12], in their local stability analysis of axisymmetric boundary layer, considered that the boundary layer develops directly on the cylindrical surface only. In all real applications like submarines, torpedoes, missiles, etc., specific shape of the forebody geometry is always used. We have considered three different forebody shapes: sharp-cone, paraboloid and ellipsoid, with FR = 2.5, 5.0 and 7.5. The boundary layer starts to develop at the stagnation point of these forebodies at a leading edge and continue on the cylindrical surface. The geometry of such forebodies develops favuorable pressure gradient while it remains constant on the cylindrical shape of the main body. The geometry of the three forebody shapes with FR = 7.5 is shown in figure 1.

Bhoraniya and Narayanan [13–15] solved two-dimensional eigenvalue problem for axisymmetric boundary layer developed on a circular cone. They found that increased semicone angle develops favourable pressure gradient and it makes the flow more stable. Bhoraniya and Narayanan [13] performed a global stability analysis of axisymmetric boundary layer developed on a circular cylinder with the hemispherical shape of the forebody. The global temporal eigenmodes are computed for different Re and azimuthal wave numbers (N) to study the spatial structure of the least stable global modes. They found that transverse curvature has a significant damping effect on the global temporal

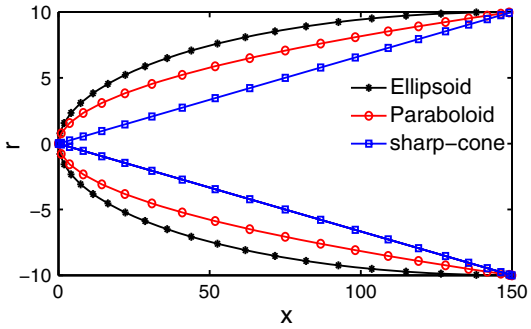

Figure 1. Schematic diagram of different axisymmetric forebody shapes (*eaf* section as shown in figure 2) with FR = 7.5. The FR is the length to diameter ratio (L/D) of the forebody shapes.

modes. Global modes for the blunt cylinder (without any forebody) and with spherical cap have been compared to investigate the impact of hemispherical forebody on an axisymmetric boundary layer. The present study is the extension of the previous work. The main aim of this paper is to study the effect of axisymmetric forebody shapes, sharp-cone, ellipsoid and paraboloid, with FR = 2.5, 5.0 and 7.5 on the stability of the boundary layer. Global modes have been analysed for these three forebody shapes.

2. Problem formulation

A circular cylinder with a as the body radius was considered in a stream of an incompressible fluid. Three different forebody shapes, namely sharp-cone, paraboloid and ellipsoid, have been considered to study their effect on the flow instabilities of an axisymmetric boundary layer developed on the cylindrical main body. The ratio of the forebody length to diameter is known as the FR. The inflow velocity component is parallel to the axis of the cylinder, and hence the base flow is axisymmetric. The fluid is incompressible with density (ρ) and kinematic viscosity (ν). The velocity and linear dimensions are normalised with the free stream velocity (U_∞) and displacement thickness (δ^*) respectively. Re of the flow is computed as

$$\mathrm{Re} = \frac{U_\infty \delta^*}{\nu}, \tag{1}$$

where δ^* is the displacement thickness at the inflow boundary of domain. The standard procedure has been adopted to derive linear stability equations for the disturbance flow quantities. The governing equations for the base flow and small disturbances are written in the cylindrical polar coordinates. Both the base flow and disturbances are axisymmetric. The instantaneous flow quantities are the sum of the base and disturbance flow quantities

$$\bar{U} = U + u, \quad \bar{V} = V + v, \quad \bar{P} = P + p. \tag{2}$$

The normal mode form is considered for infinitesimal disturbances and they are varying in the two non-homogeneous axial and radial directions respectively

$$\mathbf{q}(x, r, t) = \hat{\mathbf{q}}(x, r)\mathrm{e}^{(-i\omega t)}, \tag{3}$$

where $\mathbf{q} = [u, v, p]$, $\mathbf{Q} = [U, V, P]$ and $\bar{\mathbf{Q}} = [\bar{U}, \bar{V}, \bar{P}]$, where $\mathbf{q}$, $\mathbf{Q}$ and $\bar{\mathbf{Q}}$ are the perturbation, base and instantaneous flow quantities respectively. The governing stability equations for global stability analysis are as follows:

$$\frac{\partial u}{\partial t} + U\frac{\partial u}{\partial x} + u\frac{\partial U}{\partial x} + V\frac{\partial u}{\partial r} + v\frac{\partial U}{\partial r} + \frac{\partial p}{\partial x} - \frac{1}{\mathrm{Re}}[\nabla^2 u] = 0, \tag{4}$$

$$\frac{\partial v}{\partial t} + U\frac{\partial v}{\partial x} + u\frac{\partial V}{\partial x} + V\frac{\partial v}{\partial r} + v\frac{\partial V}{\partial r} + \frac{\partial p}{\partial r} - \frac{1}{\mathrm{Re}}\left[\nabla^2 v - \frac{v}{r^2}\right] = 0, \tag{5}$$

$$\frac{\partial u}{\partial x} + \frac{\partial v}{\partial r} + \frac{v}{r} = 0, \tag{6}$$

where

$$\nabla^2 = \frac{\partial^2}{\partial x^2} + \frac{\partial^2}{\partial r^2} + \frac{1}{r}\frac{\partial}{\partial r} = 0. \tag{7}$$

2.1 *Boundary conditions*

At the wall of a cylinder, no-slip and no-penetration conditions have been applied. Thus, all disturbance velocity components have zero magnitudes at the wall

$$u(x, a) = 0, \quad v(x, a) = 0. \tag{8}$$

In the radial direction, at a sufficiently large distance from the wall, the disturbances are expected to decay. One may consider Neumann or Dirichlet-type conditions for disturbances at free stream far away from the wall. We have considered Dirichlet-type conditions at the free stream

$$u(x, \infty) = 0, \quad v(x, \infty) = 0, \quad p(x, \infty) = 0. \tag{9}$$

To carry out global stability computations of the finite domain size, one has to truncate the numerical domain in the streamwise direction. It needs to apply artificial conditions at the outflow boundary. Thus, it is very important that the applied artificial conditions should not affect the dynamics of flow instability. Sufficiently large domain should be there to avoid any such spurious reflection at the outflow boundary. The obtained instability results depend on the type and location of the exit boundary condition. It is difficult to obtain a solution which is independent of domain size and exit boundary conditions [9,16].

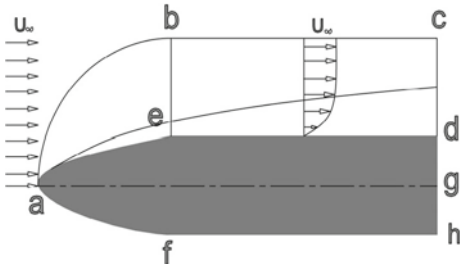

Figure 2. Schematic diagram of axisymmetric boundary layer on a circular cylinder with axisymmetric forebody. The axisymmetric domain *bcde* is used for the global instability analysis. Domain *aeb* is included in the base flow computation.

The magnitudes of the velocity disturbances have been considered zero at the inflow boundary because we are interested in studying the stability of the disturbances evolved within the domain *ebcd* shown in figure 2. Thus, it is appropriate to consider Dirichlet conditions at the inflow boundary as shown in eq. (10). The boundary conditions based on the information of leaving disturbances required to assume wave-like behaviour of the disturbances which is more restrictive in nature [17]. The streamwise wave number (α) is not known in the case of global stability analysis. The linear extrapolation-type conditions are more appropriate as it is the least restrictive. These conditions have been implemented in the global stability analysis of the boundary layer [7,8] and Channel flow [18].

$$u(x_{\mathrm{in}}, r) = 0, \quad v(x_{\mathrm{in}}, r) = 0 \tag{10}$$

$$u_{n-2}[x_n - x_{n-1}] - u_{n-1}[x_n - x_{n-2}] + u_n[x_{n-1} - x_{n-2}] = 0. \tag{11}$$

Equation (11) shows the linear extrapolation-type conditions at outflow boundary for u disturbances. Similarly, one can write for v disturbances also. As suggested by Theofilis, pressure compatibility conditions have been applied on the solid wall [7]. Lin and Malik [19,20] and Theofilis *et al* [21] have already successfully implemented it in the well-studied incompressible flow instability analysis.

$$\frac{\partial p}{\partial x} = \frac{1}{\mathrm{Re}}[\nabla^2 u] - U\frac{\partial u}{\partial x} - V\frac{\partial u}{\partial r} \tag{12}$$

$$\frac{\partial p}{\partial r} = \frac{1}{\mathrm{Re}}[\nabla^2 v] - U\frac{\partial v}{\partial x} - V\frac{\partial v}{\partial r}. \tag{13}$$

Theofilis suggested linearised pressure Poisson's equation (LPPE) for two-dimensional and three-dimensional eigenvalue problems to avoid non-physical solution [22]. Bhoraniya and Narayanan have shown that the

spectra obtained using compatibility conditions and LPPE have excellent agreement with the appropriate use of sponge region near the outflow boundary [13].

2.2 *Discretisation of stability equations*

The primitive variable approach has been used to derive the governing stability equations. The first derivative of the base flow and second derivative of the disturbances are present in the discretised equations. Lower-order derivatives are less sensitive to discretisation error than the higher-order derivatives. Chebyshev spectral collocation is used to discretise the stability equations. Spectral collocation is global and the accuracy is superior to any other discretisation scheme. So it gives better results at modest spatial resolutions with the requirement of less primary memory. The grid is generated using Chebyshev polynomial in the axial and radial directions.

$$x_c = \cos\left(\frac{\pi i}{n}\right) \quad \text{for} \quad i = 0, 1, 2, 3, \ldots, n \tag{14}$$

$$x_{\text{real}} = (1 - x_c)L_x/2 + x_{\min} \tag{15}$$

$$r_c = \cos\left(\frac{\pi j}{m}\right) \quad \text{for} \quad j = 0, 1, 2, 3, \ldots, m. \tag{16}$$

To capture the real dynamics of the flow instability in the near wall region, grid stretching is applied using the algebraic relation given by [23].

$$r_{\text{real}} = \frac{r_i L_r (1 - r_c)}{L_r + r_c(L_r - 2r_i)} + a. \tag{17}$$

Thus, the discretised equations along with boundary conditions form a general eigenvalue problem.

$$\begin{bmatrix} A_{11} & A_{12} & A_{13} \\ A_{21} & A_{22} & A_{23} \\ A_{31} & A_{32} & A_{33} \end{bmatrix} \begin{bmatrix} u \\ v \\ p \end{bmatrix} = i\omega \begin{bmatrix} B_{11} & B_{12} & B_{13} \\ B_{21} & B_{22} & B_{23} \\ B_{31} & B_{32} & B_{33} \end{bmatrix} \begin{bmatrix} u \\ v \\ p \end{bmatrix},$$

$$[A][\phi] = i\omega[B][\phi], \tag{18}$$

where A and B are square matrices of size $3 \times n \times m$, $i\omega$ is an eigenvalue and ϕ is a vector of unknown amplitude of disturbance flow quantities u, v and p.

2.3 *Solution of a general eigenvalue problem*

Equation (18) is a general eigenvalue problem. In a shear flow instability, a few least stable eigenmodes which make the flow unstable are important. So here we computed a few selected eigenmodes with largest imaginary part using Arnoldi's iterative algorithm. Readers are requested to refer [13] for the detailed discussion about the solution of the general eigenvalue problem.

3. Base flow solution

The steady Navier–Stokes equations (19)–(21) are numerically solved using the finite volume code ANSYS Fluent for an axisymmetric domain as shown in figure 2. The sharp-cone, paraboloid and ellipsoid geometries of the forebody and cylindrical geometry for the main body have been modelled with the axisymmetric domain. The FR of 2.5, 5.0 and 7.5 are considered for the geometry of the forebodies. Necessary boundary conditions are applied to close the problem. A SIMPLE algorithm with the under relaxation and quick scheme is used for spatial discretisation of the momentum equations. The grid conversion study is presented in table 1 to show that the base flow solution is independent of the considered grid size.

The convergence of the base flow solution is also tested by computing the residual of the mass conservation ($\nabla \cdot \mathbf{U}$) over the entire axisymmetric domain. It has been found that the residual of the mass conservation reduces with the increased grid size as shown in table 1.

Thus, the obtained velocity profile in the axisymmetric domain has been interpolated to the spectral grid using cubic spline interpolation to perform stability analysis.

$$U\frac{\partial U}{\partial x} + V\frac{\partial U}{\partial r} = -\frac{\partial P}{\partial x} + \frac{1}{\text{Re}}\left(\frac{\partial^2 U}{\partial x^2} + \frac{1}{r}\frac{\partial U}{\partial r} + \frac{\partial^2 U}{\partial r^2}\right) \tag{19}$$

$$U\frac{\partial V}{\partial x} + V\frac{\partial V}{\partial r} = -\frac{\partial P}{\partial r} + \frac{1}{\text{Re}}\left(\frac{\partial^2 V}{\partial x^2} + \frac{1}{r}\frac{\partial V}{\partial r} + \frac{\partial^2 V}{\partial r^2}\right) \tag{20}$$

$$\frac{\partial U}{\partial x} + \frac{\partial V}{\partial r} + \frac{V}{r} = 0. \tag{21}$$

The forebody shape generates favourable pressure gradient in the streamwise direction. However, the pressure gradient remains constant in the flow direction on the main body (cylinder).

3.1 *Effect of forebody shape on the base flow profile*

Figures 3 and 4 show the comparison of the base velocity components U and V for sharp-cone, paraboloid

Table 1. The grid convergence study for the base flow is obtained, using U (50, 1.4) and V (50, 1.4) for Re = 230. The successive grid refinement ratio in both the directions is 1.4142. The relative error was computed using two consecutive grid sizes. The convergence of the solution is also tested by computing the residual of mass conservation over the entire axisymmetric domain ($\nabla \cdot \mathbf{U}$) for mesh #1, #2 and #3.

Mesh	Grid size	U	ϵ (%)	V	ϵ (%)	$\nabla \cdot \mathbf{U}$
#1	2001×251	0.163016	0.027	0.00020735	0.005	8.220×10^{-8}
#2	1415×177	0.162972	0.049	0.00020734	0.01	2.067×10^{-7}
#3	1001×125	0.162894	–	0.00020732	–	2.245×10^{-6}

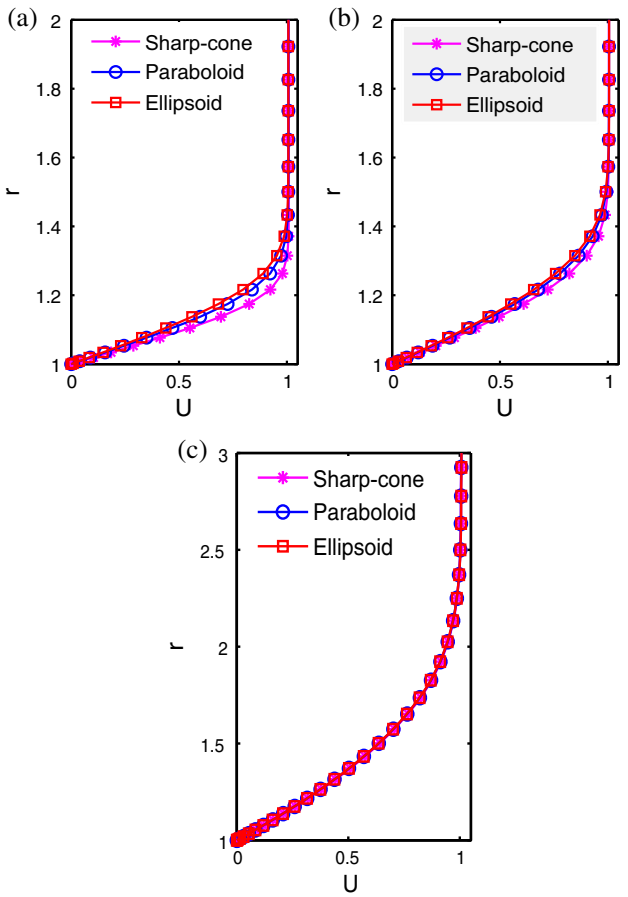

Figure 3. Effect of different forebody geometries on the axial velocity (U) for Re = 230 at different streamwise locations, (**a**) $x = 3$, (**b**) $x = 5.5$ and (**c**) $x = 50$. The domain size in the wall normal direction is taken as 20 times the cylinder radius.

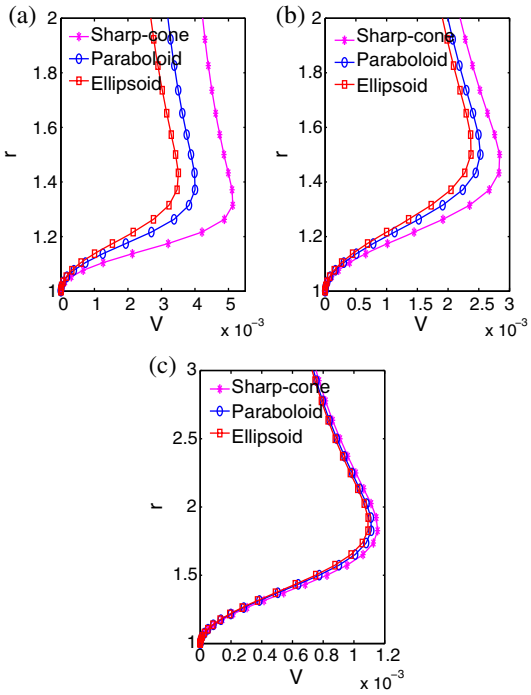

Figure 4. Effect of different forebody geometries on the radial velocity (V) for Re = 230 at different streamwise locations, (**a**) $x = 3$, (**b**) $x = 5.5$ and (**c**) $x = 50$. The domain size in the wall normal direction is taken as 20 times the cylinder radius.

and ellipsoid geometries as the forebody at different streamwise stations. Near the leading edge, the forebody geometry affects the base velocity profile. However, this effect reduces gradually towards the downstream in the flow direction. Similarly, the non-parallel effects are higher near the leading edge for the sharp-cone shape. However, it is the same for all the three geometries towards the downstream side. The transverse curvature (ratio of boundary layer thickness to body radius of cylinder, δ/a) and shape factor have significant difference near the leading edge region and gradually reduces towards the downstream as shown in figures 5a and 5b. This indicates that the velocity profile and growth of the boundary layer, and subsequently the stability of the boundary layer, are mostly affected by different forebody geometries near the leading region. Figure 5a shows that favourable pressure gradient (acceleration) effect is highest for sharp-cone geometry and least for ellipsoid geometry. Similar tendency has been found for the radial ($\partial U/\partial r$, $\partial^2 U/\partial r^2$) and axial ($\partial U/\partial x$) derivatives for the forebody geometry as shown in figures 6 and 7. The difference in non-parallel effects are found significant near the leading edge of a cylinder, and gradually it reduces in the flow direction. In summary, the forebody shapes have significant effects on the

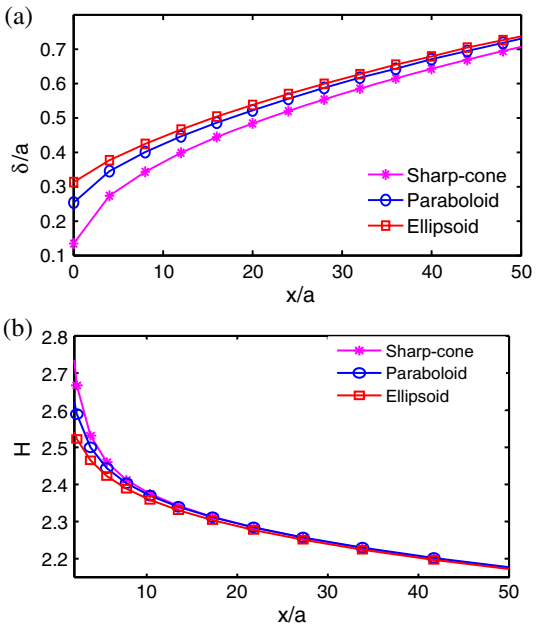

Figure 5. Variation of the (**a**) transverse curvature (δ/a) and (**b**) shape factor (H) in the streamwise direction for Re = 230 and different forebody shapes.

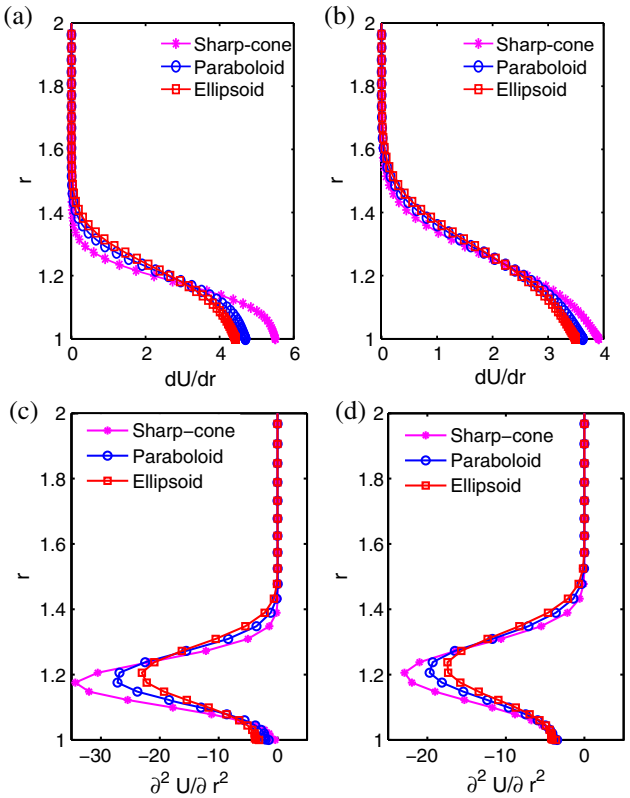

Figure 6. Effect of different forebody geometries at Re = 230 and different streamwise locations on $\partial U/\partial r$ at (**a**) $x = 3$, (**b**) $x = 5.5$ and on $\partial^2 U/\partial r^2$ at (**c**) $x = 3$ and (**d**) $x = 5.5$. The domain size in the wall normal direction is taken as 20 times the cylinder radius.

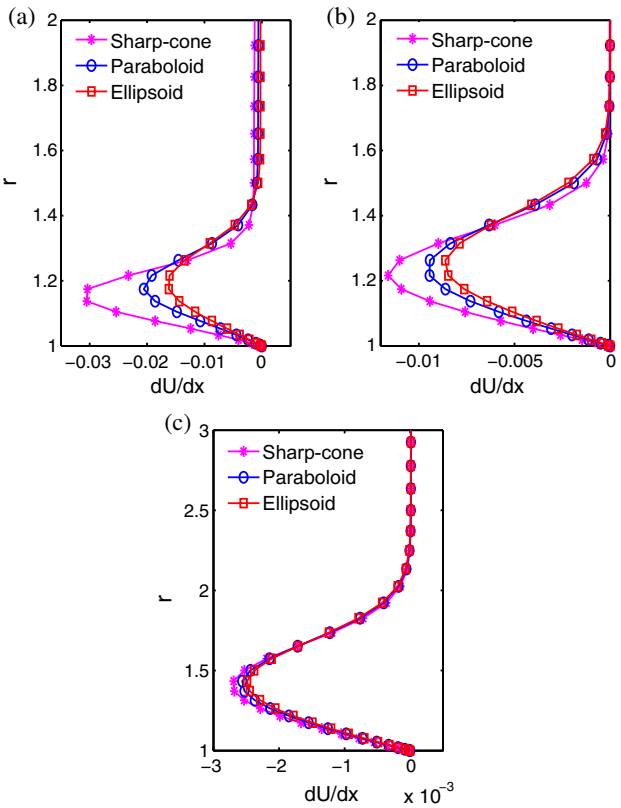

Figure 7. Effect of different forebody geometries on dU/dx for Re = 230 at different streamwise locations, (**a**) $x = 3$, (**b**) $x = 5.5$ and (**c**) $x = 50$. The domain size in the wall normal direction is taken as 20 times the cylinder radius.

characteristics of the base flow at the leading edge of the boundary layer, i.e. non-parallel effect, transverse curvature, pressure gradient and boundary layer thickness.

3.2 *Effect of FR on the base flow profile*

Three different forebody geometries have been selected for the stability analysis. Figure 8 shows the comparison of V for three different FRs when the shape of forebody is paraboloid. The magnitude of V is found higher near the leading edge. However, at $x = 50$ the magnitude is almost the same for FR = 2.5, 5.0 and 7.5. At $x = 5$, FR = 2.5 has larger value of V indicating higher non-parallel effects. Similarly, the derivative dU/dr is also higher at $x = 5$ for FR = 2.5 and at $x = 50$ it is the same for FR = 2.5, 5.0 and 7.5. The study of the base flow with different geometries of the forebody and with different FRs shows that the effect of different shapes has a significant influence on the base flow at leading edge only. The base flow velocity profile is almost the same towards downstream in the flow direction (figure 9).

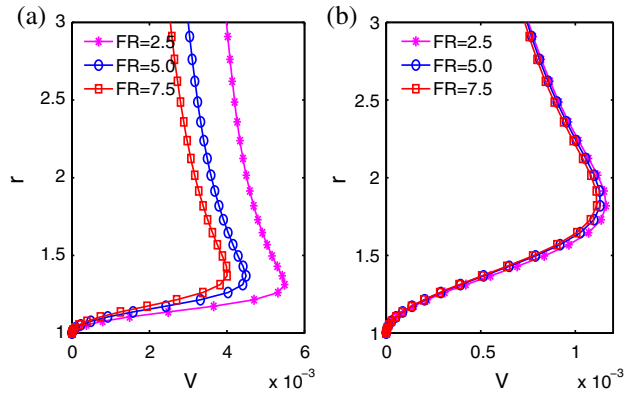

Figure 8. Effect of FR on V for Re $= 230$ at different streamwise locations, (**a**) $x = 5$ and (**b**) $x = 50$.

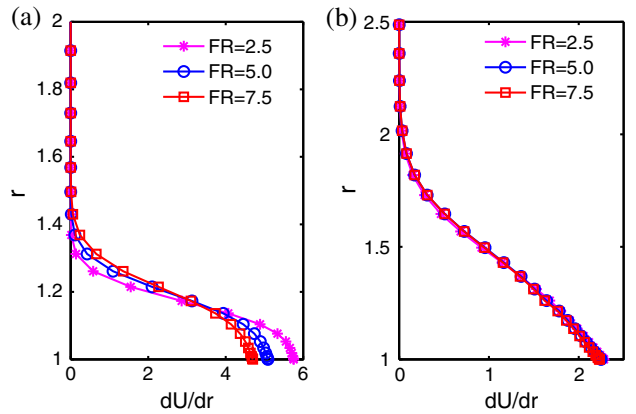

Figure 9. Effect of FR on $\mathrm{d}U/\mathrm{d}r$ for Re $= 230$ at different streamwise locations for the paraboloid geometry. (**a**) $x = 5$ and (**b**) $x = 50$.

4. Results and discussions

In the present instability analysis, a domain length of 400 and inlet Re $= 230$ are considered. Re is computed based on the displacement thickness at the inflow boundary of the domain. It has been found from the analysis of the base flow that the effect of forebody geometry is significant near the leading edge of the cylinder only and towards the downstream the velocity profile for different forebody shapes are almost similar. Thus, the domain length of 400 is sufficient to study the effect of forebody geometries on the stability characteristics of the boundary layer. The domain size of $20\delta^*$ considered in the normal wall direction, is sufficient to apply the freestream condition. The number of collocation points considered in the axial and radial directions are 221 and 61. The forebody shapes like sharp-cone, paraboloid and ellipsoid are considered to study their effects on the flow stability of the main body (cylinder) as shown in figure 1. Thus, the forebodies are considered in base-flow computations only. A hyperbolic tangent function as shown by eq. (22) is used for applying to sponge near the outflow boundary towards downstream to prevent any spurious reflection at the outflow boundary.

$$\mathrm{Re}_{\mathrm{sponge}} = \mathrm{Re}\left[1 - \frac{1 - S_{\mathrm{sponge}}}{2}(1 + \tanh(\theta))\right], \quad (22)$$

where

$$\theta = 2\pi\left[\frac{x - x_{\min}}{L_{\mathrm{s}}} - 0.5\right],$$

S_{sponge} is the sponging strength in %, L_{s} is the sponging length in % of the total domain length and $x_{\min}$ is the streamwise location from where sponging is applied. If sponging strength and sponging length are 20 and 30% respectively, then outflow Re reduces to 20% of the flow Re over 30% of the exit domain length. It has been shown that results obtained are not affected due to the sponge region. The two-dimensional eigenvalue problem was solved using ARPACK which uses Arnoldi's algorithm. Authors have already validated the global stability results against the local stability analysis [13].

4.1 *Grid convergence test*

A grid convergence study has been perfomed for a paraboloid forebody with FR $= 5.0$ to check the proper grid size and grid independancy of the obtained results. The grid convergence study is reported in table 2. Two leading eigenmodes have been observed for three different grid sizes for Re $= 230$ for axisymmetric mode $N = 0$. A refinement ratio of 1.142 is adopted in the axial and radial directions to improve spatial grid resolution. The monotonic behaviour of the real and imaginary parts of the eigenvalues have been found with improved resolution. The relative errors were computed for the real and imaginary parts of the eigenvalue, and the largest one is reported in the table. As shown in table 2, grid #1 has been used in the reported stability computations.

4.2 *Axisymmetric modes* ($N = 0$)

4.2.1 *Effect of forebody shapes on global temporal modes.* The three different forebody geometries are considered to study their effects on the stability of the boundary layer. The families of eigenspectrum for Re $= 230$, $N = 0$, FR $= 5.0$ and domain length $Lx = 400$ are shown in figure 10. The comparison of the discrete part of the spectrum is only presented here. The domain length is the same for all the four body shapes. Figure 10 shows that temporal growth rate is highest for the ellipsoid shape and lowest for the blunt cylinder and sharp-cone shapes. The difference in the temporal growth rate found between the sharp-cone, paraboloid

Table 2. The grid convergence study for two least stable eigenmodes ω_1 and ω_2 for Re = 230, axisymmetric mode $N = 0$, paraboloid forebody with FR = 5.0 and three different grid sizes. The grid refinement ratio of 1.142 is used to improve the resolution in the axial and radial directions. The maximum absolute error (ϵ) is shown here. The domain sizes, *Lx* and *Lr*, are 400 and 20 respectively.

Mesh	*Lx*	*Lr*	$n \times m$	n	m	ω_1	ω_2	ϵ (%)
#1	400	20	13481	221	61	0.00185–0.01601i	0.00633–0.01925	2.315
#2	400	20	10229	193	53	0.00188–0.01690i	0.00647–0.01938	4.082
#3	400	20	8037	171	47	0.00196–0.01675i	0.00669–0.01985	–

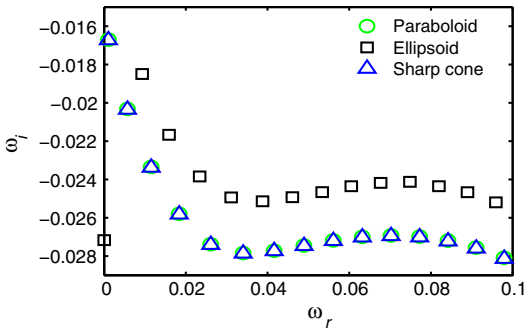

Figure 10. Comparison of the eigenspectrum for different forebody shapes for $N = 0$, Re = 230 and FR = 5.0.

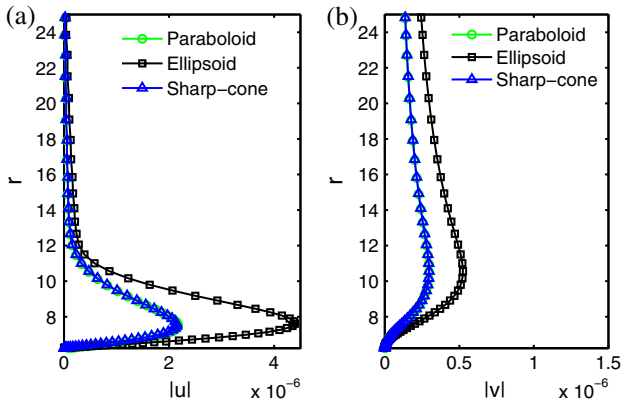

Figure 11. Comparison of the spatial eigenmodes at the streamwise location $x = 200$ for FR = 5.0, $N = 0$ and Re = 230 for different forebody shapes.

and blunt cylinder are too small. However, the difference of temporal growth rate between the ellipsoid and the remaining shapes are comparatively large. The overall comparison of the spectrum for FR = 2.5, 5.0 and 7.5 demonstrates that an increased FR damps the temporal growth rate.

Figure 1 shows that the sharp-cone and paraboloid forebodies are sharper than the ellipsoid forebody. Thus, the sharp-cone and paraboloid geometries develop more favourable pressure gradient in the streamwise direction than the freebody with the ellipsoid geometry. It is well known that more favourable pressure gradient makes the flow temporally more stable. Thus, the boundary layer developed on the elliptical forebody is less stable. However, the global modes have been found stable for all the three forebody shapes. Figures 6c and 6d show the comparison of $\partial^2 U/\partial r^2$ at $x = 3.5$ and 5.5 for different forebody shapes. It is found that the negative values of $\partial^2 U/\partial r^2$ is highest for sharp-cone and lowest for ellipsoid forebody. It is well known that larger negative values of $\partial^2 U/\partial r^2$ make the flow more stable. Thus, these characteristics of the base flow makes the boundary layer more stable with sharp-cone and least stable for elliptical forebody.

The comparison of the discrete part of the spectrum is only presented here. The domain length is the same for all the cases. Figure 10 shows that temporal growth rate for the ellipsoid forebody is highest among all and it is the lowest for the boundary layer with the blunt cylinder and sharp-cone forebody. The difference in the temporal growth rate between the sharp-cone, paraboloid and blunt cylinder are too small. However, the difference of temporal growth rate between the ellipsoid and the remaining geometries are comparatively large. The overall comparison of the spectrum for FR = 2.5, 5.0 and 7.5 demonstrates that an increase in FR damps the temporal growth rate.

To evaluate the spatial growth rate of the eigenmodes of the boundary layer with different forebody shapes, the least stable temporal eigenmodes are selected from the spectra. Figure 11 shows the comparison of the eigenfunctions at the streamwise location $x = 400$. The disturbance amplitude functions for the ellipsoid forebody has the largest magnitude, and that of the blunt cylinder has the least one. Thus, it proves that the axisymmetric boundary layer with the ellipsoid forebody geometry is temporally and spatially the least stable one while that of a blunt cylinder is the most stable. To compute the growth of all the disturbances together in the streamwise direction, a spatial growth rate (A_x) is computed as shown in figure 12. The spatial growth for the ellipsoid forebody is found highest among all forebodies.

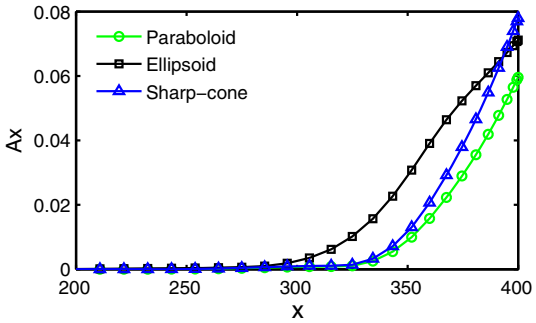

Figure 12. Comparison of the spatial eigenmodes at the radial location $r = 1.4$ for FR $= 5.0$, $N = 0$ and Re $= 230$ for different forebody shapes.

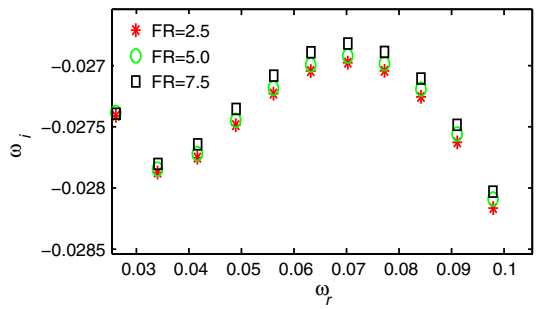

Figure 13. Comparison of eigenspectrum for $N = 0$ and Re $= 230$ with different FR for the paraboloid forebody.

$$A(x) = \sqrt{\int_1^{r_{\max}} (u^*(x,r)u(x,r) + v^*(x,r)v(x,r))\mathrm{d}r}. \tag{23}$$

4.2.2 *Effect of FR on temporal global modes.* In this section, the temporal and spatial properties of the eigenmodes are discussed with different FRs. Figure 13 shows the comparison of the eigenspectrum for paraboloid forebody with Re $= 230$ and different FR. The domain length considered is the same for all FRs. The distribution of the frequency is found to be almost the same for each case. However, the temporal growth rate is found higher with FR $= 7.5$ and lower with FR $= 2.5$. Thus, increasing FR increases the temporal growth rate of eigenmodes for the paraboloid forebody. The sharpness of the given forebody is higher with small FR, which gives larger favourable pressure gradient effect, resulting in the lower temporal growth of the disturbances. The least stable eigenmode for each FR is selected, and the corresponding eigenfunctions are compared with each other at the streamwise location $x = 200$. It has been found that the eigenfunction for FR $= 5.0$ has the least spatial growth (figure 14).

Figure 15 presents the eigenspectrum for Re $=$ 230 with different FR for the ellipsoid geometry. The

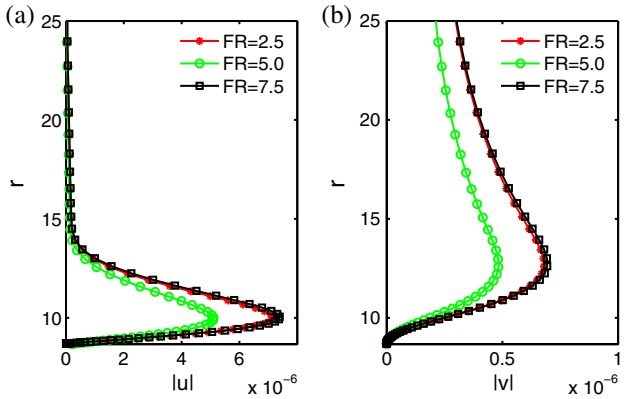

Figure 14. Comparison of the spatial eigenmodes at streamwise location $x = 200$ for $N = 0$ and Re $= 230$ with different FR for the paraboloid forebody.

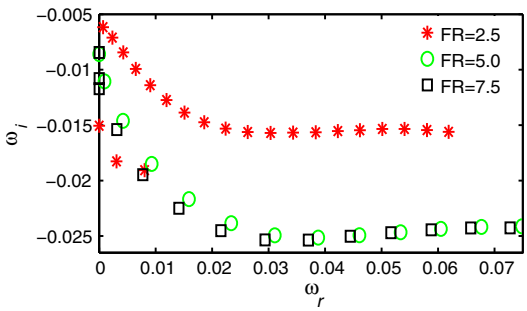

Figure 15. Comparison of eigenspectrum for $N = 0$ and Re $= 230$ with different FR for the ellipsoid forebody.

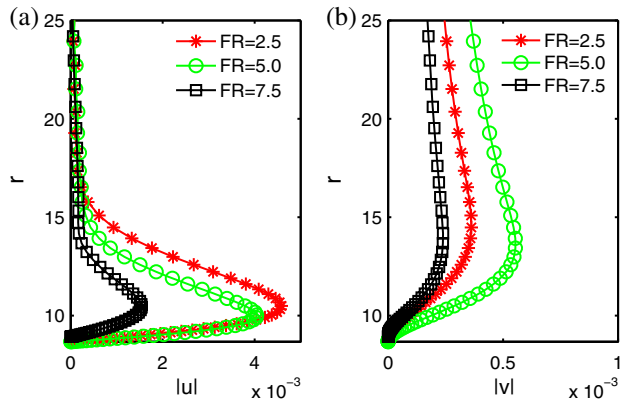

Figure 16. Comparison of the spatial eigenmodes at streamwise location $x = 280$ for $N = 0$ and Re $= 230$ for the paraboloid forebody.

temporal growth is the highest for FR $= 2.5$ and the lowest for FR $= 7.5$. The temporal growth rate reduces with the increase in FR. The comparison of the spatial eigenmodes shown at $x = 200$ is shown in figure 16 for ellipsoid geometry. It is found that the spatial growth rate of the eigenmodes is highest for FR $= 2.5$ and lowest for FR $= 7.5$. Thus, the temporal and spatial growth

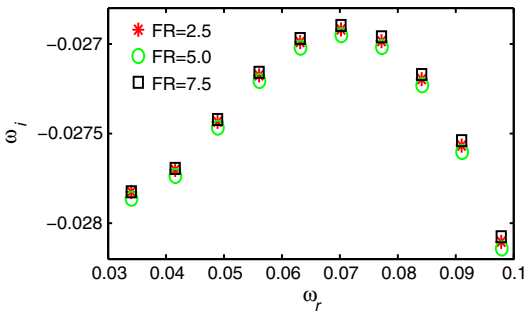

Figure 17. Comparison of eigenspectrum for $N = 0$ and $\mathrm{Re} = 230$ with different FRs for the sharp-cone forebody.

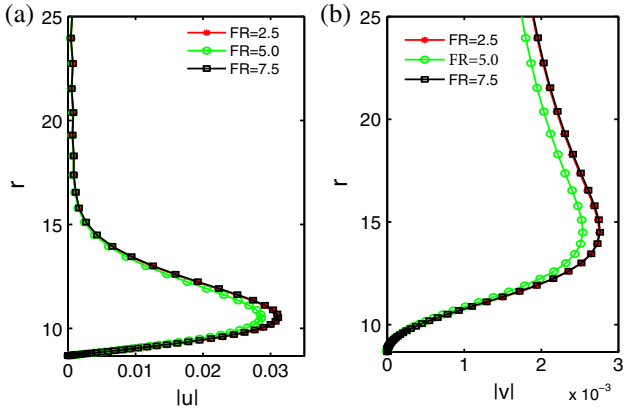

Figure 18. Comparison of the spatial eigenmodes at streamwise location $x = 280$ for $N = 0$ and $\mathrm{Re} = 230$ for the sharp-cone forebody.

for different FRs found here is different from that of the paraboloid forebody. The small FR (2.5) increases the bluntness of the ellipsoid forebody which develops less favourable pressure gradient resulting in larger temporal growth of disturbances. Figure 17 shows the comparison of eigenspectrum for sharp-cone forebody. The temporal growth rate is found least with FR = 5.0 and highest with FR = 2.5. The comparison of the eigenfunctions also shows similar trends. The spatial growth of amplitude functions are nearly the same for FR = 2.5 and FR = 7.5 and FR = 5.0 is the least one. Thus, for different FRs, different temporal and spatial characteristics are found (figure 18).

5. Summary

Linear stability theory has been applied to perform global stability analysis of the axisymmetric boundary layer developed on a circular cylinder with different axisymmetric forebody shapes. Forebodies with sharp-cone, paraboloid and ellipsoid geometries with FR = 2.5, 5.0 and 7.5 have been considered to analyse the effect of geometry on the temporal and spatial stability of the boundary layer. The two-dimensional eigenvalue problem has been numerically solved using Arnoldi's iterative algorithm for the axisymmetric modes of disturbances.

It has been found that forebody shapes and FR have significant influence on the base flow velocity near the leading edge of the boundary layer. However, the effect forebody shape reduces towards downstream in boundary layer and at $x = 50$ the velocity profile is almost the same for all the three forebody shapes.

The sharp-cone geometry has the most significant influence on the radial and streamwise derivatives near the leading edge, showing substantial non-parallel effects compared to paraboloid and ellipsoid forebodies.

The computed global eigenmodes are temporally stable because all eigenvalues have a negative imaginary part (ω_i). The computed temporal global modes are found the least stable for ellipsoid forebody and the most stable for the sharp-cone forebody for given values of Re and FR. Similar trends have been observed for the spatial growth rate of the least stable global modes in the streamwise direction. The global modes of paraboloid and sharp-cone are found the least stable at FR = 7.5 while that of ellipsoid are found at FR = 2.5. The marginal difference has been found in the temporal growth rate for the paraboloid and sharp-cone geometries. However, the temporal growth of ellipsoid geometry has been found large compared to paraboloid and sharp-cone shape. The stability results presented depend on the streamwise extent of the domain.

References

[1] J S Parsons and R E Goodson, *Technical report H*, Automatic Control Center, School of Mechanical Engineering (Purdue University, 1972)
[2] V Narayanan and R Govindarajan, *Pramana – J. Phys.* **64**(**3**), 323 (2005)
[3] M Casarella, T C Shen and B E Bowers, *Ship Acoustic Dept. R & D Report* **77** (1977)
[4] R L James, B H Navran and R A Rozenddal, NASA CR-166051 (1984)
[5] B J Holmes, C J Obara and L P Yip, NASA TP-2256 (1984)
[6] B H Carmichael, *Underwater missile propulsion* (Compass Publications, 1966)
[7] V Theofilis, *Prog. Aerosp. Sci.* **39**, 249 (2003)
[8] F Alizard and J C Robinet, *Phys. Fluids* **19**, 114105 (2007)
[9] E Akervik, U Ehrenstein, F Gallaire and D S Henningson, *Eur. J. Mech. B/Fluids* **27**, 501 (2008)
[10] G N V Rao, *J. Appl. Math. Phys.* **25**, 63 (1974)
[11] O R Tutty and W G Price, *Phys. Fluids* **14**, 628 (2002)
[12] V Narayanan, *Stability and transition in boundary layer: Effect of transverse curvature and pressure gradients*, Ph.D. thesis (Jawaharlal Nehru Centre for Advanced Scientific Research, Bangalore, 2005)

[13] R Bhoraniya and V Narayanan, *Theor. Comput. Fluid Dyn.* **32**, 425 (2018)
[14] R Bhoraniya and V Narayanan, *J. Phys.: Conf. Ser.* **822**, 012018 (2017)
[15] R Bhoraniya and V Narayanan, *Phys. Rev. Fluids* **2**, 063901 (2017)
[16] U Ehrenstein and F Gallaire, *J. Fluid Mech.* **536**, 209 (2005)
[17] H Fasel, U Rist and U Konzelmann, *AIAA J.* **28**, 29 (1990)
[18] G Swaminathan, K Shau, A Sameen and R Govindarajan, *Theor. Comput. Fluid Dyn*. **25**, 53 (2011)
[19] R S Lin and M R Malik, *J. Fluid Mech.* **311**, 239 (1996)
[20] R S Lin and M R Malik, *J. Fluid Mech.* **333**, 125 (1997)
[21] V Theofilis, P W Duck and J Owen, *J. Fluid Mech.* **505**, 249 (2004)
[22] V Theofilis, *Theor. Comput. Fluid Dyn.* **31**, 623 (2017)
[23] M R Malik, *J. Comput. Phys.* **86**(**2**), 372 (1990)